5-2016

Changes in Expression of Innervation and Accompanying Epithelium within Sjögren's Syndrome NOD/ShiLtJ Mouse Model

Nicholas Pagendarm
University at Albany, State University of New York

Changes in Expression of Innervation and Accompanying Epithelium within Sjögren's Syndrome NOD/ShiLtJ Mouse Model

An honors thesis presented to the Department of Biological Sciences,

University at Albany, State University of New York

in partial fulfillment of the Honors Program Requirements.

Nicholas Pagendarm

Spring 2016

Mentors: Dr. Melinda Larsen

Kara DeSantis

Department of Biological Sciences
University at Albany

This Honors Thesis has been read and approved by the undersigned and is hereby recommended for acceptance.

Thesis Committee:

Research Advisor:

Melinda Larsen _____ 5/3/16

(Name) (Signature) (Date)

Committee Member:

PRASHANTH RANGAN _____ 5/3/16

(Name) (Signature) (Date)

ACTION: Accepted ☑ Not Accepted ☐

_____ 5/3/16

Departmental Honors Program Director Date

ABSTRACT

The salivary gland produces saliva that aids in digestion and in maintaining homeostasis in the oral cavity. Saliva production is disrupted in Sjögren*'s* Syndrome (SS), where the salivary gland is attacked by the immune system, leading to loss of function and hyposalivation. SS is thought to be accompanied by changes in the salivary epithelium, which are incompletely understood. In this study we have used the non-obese diabetic (NOD) mouse as a model for SS to study the changes in salivary gland epithelium, as these models present autoantibodies and other characteristics such as immune infiltrates similar to those found in SS patients. To quantify and explore glandular changes in both mouse and human tissue, epithelial proteins marking specific cell types were compared using multiplexed immunohistochemistry and immunofluorescent microscopy. Epithelial markers were characterized in human SS and two types of human control tissue, autopsy, and non-SS biopsies, and these results were compared to NOD epithelial tissue and healthy CD-1 age-matched controls. Specific protein markers used included cytokeratin 7 for ductal cells, cytokeratin 5 for undifferentiated progenitor cells, aquaporin 5 (AQP5) for acinar cells, smooth muscle α-actin for myoepithelial cells, and a small panel of innervation specific markers. In order to determine the effect of disease progression over time on the submandibular salivary epithelium, protein level and localization were compared between SS-like NOD tissue and CD-1 age-matched control tissues. Changes in protein levels were quantified using specialized quantitative immunohistochemistry, incorporating newly developed protocols. In order to evaluate the efficacy of the NOD mouse model as a model for human disease, mouse tissues were compared to human SS and control

tissues. We conclude that while SS-like disease progression in the NOD mouse model occurs over time, the phenotype of the gland at time points previously characterized as late-stage disease may represent an earlier phenotype of diagnosed human SS, which is typically detected at a late stage.

TABLE OF CONTENTS

INTRODUCTION

Sjögren's Syndrome (SS) is a chronic autoimmune disease that targets the salivary and lacrimal glands, resulting in a progressive loss of salivary secretion (Gao 2006). Loss in exocrine function is often undetected until there has been a significant decrease. Clinical presentation of SS in humans is characterized by the presence of xerostomia (dry mouth) and keratoconjunctivitis sicca (dry eyes) (Venables 2004). These disease manifestations can be debilitating to patients, who are forced for the duration of their life to use synthetic over-the-counter eye drops and mouth preparations to simulate tears and saliva. In addition, there are prescription medications to help combat dry eyes, dry mouth, and the systemic manifestations. These medications can help to lessen symptoms, but do not directly treat the disease (Sjögren's Syndrome Foundation April 2014). There is currently no cure for SS.

Diagnosis and Prevalence of Sjögren's Syndrome

SS is one of the most prevalent autoimmune diseases in the United States (as reviewed in Fox 2007). The National Arthritis Data Workgroup indicates that the presence of SS has been estimated at 1.3 million cases out of the approximate population of 214.8 million within the United States. Out of these cases, the ratio of instances for women to men is 9:1, indicative of a possible correlation between disease expression and gender (as reviewed in Lavoie 2011), although other research suggests that the female to male ratio may be closer to 20:1 (Westhoff 2010). Part of the reason for the uncertainty is the difficulty in diagnosing SS and the changing criteria. The criteria currently proposed by the American College of Rheumatology (ACR) for SS diagnosis includes the expression of 2 out of 3 manifestations that are necessary to be present

for a diagnosis. These diagnostic criteria include an ocular surface damage test, a blood test positive for certain SS associated antibodies, and a salivary gland biopsy positive for lymphocytic infiltrates (Shiboski 2012). Since Sjögren's Syndrome is often expressed along with other autoimmune diseases such as rheumatoid arthritis, or systemic lupus erythematosus (Tincani 2013), which is known as secondary Sjögren's Syndrome, it can be difficult to diagnose and to study.Considering the large number of individuals affected by SS, it is important to find effective, long-lasting treatments to improve the quality of life for these individuals.

Use of the NOD/ShiLtJ Mouse Model for the Study of Sjögren's Syndrome

In order to study SS in the laboratory, mouse models are used, including the non-obese diabetic (NOD/ShiLtJ) model (Jonsson 2006, Lavoie 2011). The NOD/ShiLtJ mouse model is useful for study of SS due to the presence of the SS phenotype including reduced salivary and lacrimal production accompanied by lymphocytic infiltrate. Both human SS patients and the NOD/ShiLtJ mouse model develop disease-characteristic lymphocytic infiltrates increasing in prevalence and size with disease progression. Lymphocytic infiltrates found in both the salivary and lacrimal glands have been found to contain T cells and macrophages (Venables 2004, Lavoie 2011). These lymphocytic cells within the infiltrates may target specific proteins within these glands, and could be a causative factor in the loss of function that results from disease progression. Lymphocytic infiltration onset in the salivary and lacrimal glands of the NOD/ShiLtJ model occurs at approximately 12 weeks of age and is present at approximately 16-20 weeks of age, resulting in a loss of exocrine function by 20 weeks (Lavoie 2011).

As in humans, SS-like symptoms in the NOD/ShiLtJ model are accompanied by the detectable presence of specific autoantibodies, including autoantibodies to nuclear proteins, namely anti-Ro/SS-A, and anti-La/SS-B, and are correlated with secretory dysfunction. Other autoantibodies, including autoantibodies that target innervation receptors, such as muscarinic receptor 3 and beta adrenergic receptor, enhance the similarity between the NOD/ShiLtJ model and clinical presentation as they are also present in SS human patients. Anti-muscarinic receptor 3 may also be a potential influence on secretory dysfunction within both human SS patients and the animal model, possibly through the blocking of neurotransmission through this receptor (Venables 2004). Although the presence of autoantibodies and lymphocytic infiltrates may play a large role in the development of SS in the NOD/ShiLtJ mouse model, other causative factors thought to play a role in the development of SS in humans may also be factors in contributing to development of disease such as previous systemic viral infection and epigenetic changes (Venables 2004). In addition to similar immune system characteristics between human SS patients and the NOD/ShiLtJ mouse model, the mouse model also exhibits similar gender differences in presentation, with the females expressing salivary symptoms earlier than males by a matter of weeks. This correlates to the sexual dimorphism observed in clinical presentation of SS in humans. Since the NOD/ShiLtJ mouse model is extremely similar to human SS in both autoantibodies present and clinical presentation, the model should be an excellent vehicle for studies and research work involving SS (Lavoie 2011).

The Epithelium of the Salivary Gland Changes in Sjögren's Syndrome

In the salivary gland, epithelial acinar cells organized in a spherical structure secrete saliva, facilitated by the myoepithelial cells which surround them. The myoepithelial cells contract, squeezing the acinar cells, which then release the saliva into the hollow lumen located in the center of the acinar units (Holmberg 2014 and Tucker 2007). This secretion is released from vesicles in the acinar cells and travels through the lumen, which is continuous with the ductal network. This allows the saliva to travel through the salivary gland to the oral cavity as the ductal cells modify it so that it is capable of performing all of the needed functions. During disease progression in SS, changes within the salivary gland occurring with disease progression and loss of function have been examined, including a global increase in the ductal epithelium (Ihrler 2000, Konttinen 2006) which is required for saliva transport from the gland. In humans, atrophy of aquaporin 5 (Aqp5)-positive secretory acinar epithelium is thought to occur in SS (Daniels 1984), along with dysregulation of innervation (Konttinen 2006), suggesting a loss in capability of saliva production and secretory ability.

The Role of Innervation in the Salivary Gland

Autonomic innervation within the salivary gland has been shown to play a large part in both tissue development and the regenerative capabilities of the gland. Neuronal-epithelial interactions are important in submandibular gland (SMG) salivary function in animal models (Ferreira 2013). The two subtypes of autonomic innervation, sympathetic and parasympathetic, are thought to influence both tissue development and the regenerative capabilities of the salivary glands differently. It is suggested that both parasympathetic and sympathetic

innervation play roles in the development of the gland, with parasympathetic innervation influencing glandular development prior to birth and sympathetic innervation influencing specifically the development and differentiation processes of mature acinar and ductal cells postnatally (Proctor 2007).

Parasympathetic innervation is important for regeneration and homeostasis of the salivary gland. During regeneration, the importance of parasympathetic innervation can be observed in a ductal ligation model where glands that showed no parasympathetic functionrecovered to only approximately 60% of stimulated secretory functionality compared to those that were normally innervated (Proctor 2007). Also, in an irradiation model of regeneration, it was observed that decreased levels of parasympathetic innervation due to irradiation are correlated with a decreased regenerative capability of salivary glands, whereas normal or increased levels of parasympathetic innervation promotes tissue regeneration after irradiation (Knox 2013). Parasympathetic innervation is not only important for function, it is also important for development. A study from Knox, et al. showed a necessity for parasympathetic innervation in maintenance of the K5-positive progenitor cells during development (Knox 2010). In the future, manipulation of the balance of innervation within the gland in order to influence the K5 positive progenitor pool could provide a potential form of treatment for clinical patients suffering from hyposalivation as well as other forms of salivary gland dysfunction. Within the salivary gland tissue of individuals suffering from SS, these changes in progenitor cells due to aberrant innervation and function could also contribute to the loss of function that occurs.

Examination of Epithelial and Innervation Changes in the NOD/ShiLtJ Mouse Model of Sjögren's Syndrome

In this study, to characterize the phenotypic differences in innervation and epithelial markers between human SS patients and the NOD/ShiLtJ model, we used quantitative immunohistochemical staining and imaging. ***We hypothesized that the NOD/ShiLtJ mouse model for SS would mimic the phenotypic changes reported in human SS patients during SS disease progression.*** In order to examine these phenotypic changes through disease progression in the NOD/ShiLtJ mouse model as compared to CD-1 control age-matched control mice, we examined multiple markers in the submandibular salivary gland (SMG) at the 12, 18, and 22 week time points using a tissue microarray. Based on prior studies, these specific time points were chosen to be representative of early, mid, and late disease in the female mice. We developed and employed a new method of image processing and quantitative immunohistochemistry to assess the degree of change in the NOD/ShiLtJ model as compared to control. We examined phenotypic structural differences known to occur in human SS patient salivary tissue, such as an increase in ductal quantity (Konttinen 2006), that can be marked and quantified using specific markers, such as cytokeratin 7 (K7) (Nelson 2013), in order to validate our quantification method. In order to examine the epithelium we used markers for K7, marking ducts, AQP5, marking acinar epithelium, (SMα-A), marking myoepithelium, and sodium potassium ATPase (Na/K-ATPase), highlighting total salivary epithelial tissue. In order to examine innervation within the gland, βIII tubulin (βIII) was used to mark total innervation, while tyrosine hydroxylase (TH) and Gfrα-2 were used to identify sympathetic innervation and parasympathetic innervation, respectively. Since it is known that increased sympathetic

innervation can result in decreased ability of SMG regeneration (Knox 2013), we chose to examine the epithelial progenitor marker K5 in order to determine if this population was reduced in the NOD/ShiLtJ model as compared to control. Both parasympathetic and sympathetic innervation are thought to influence SMG regeneration independently and differently, so it is important to examine both types of innervation and compare their levels and localization in this study. Since innervation is thought to be dysregulated in human SS (Konttinen 2006), we examined both parasympathetic and sympathetic innervation in order to determine any differences in ratio or levels expressed between the CD-1 control mouse and NOD/ShiLtJ mouse model during disease progression.

MATERIALS AND METHODS

Immunohistochemistry Using Formalin-Fixed, Paraffin Embedded Tissues in a Microarray

In order to examine both mouse and human tissues, tissue microarrays (TMAs) were constructed from paraffin embedded samples. Mouse TMAs were constructed using 104 randomly placed spots per slide consisting of 18 and 22 week CD-1 and NOD/ShiLtJ submandibular salivary tissues and other staining control tissues including postnatal SMG, smooth muscle and thymus. Human labial gland biopsies obtained from the University of Oslo, Norway. Human TMAs were constructed using 39 spots of human samples and included an additional four mouse CD-1 tissue spots for staining controls. In order to prepare paraffin TMAs for staining and imaging, they were first deparaffinized, followed by an antigen retrieval step prior to antibody application, and imaging of the tissue to examine the fluorescence. Prior to deparaffinization, the 0.5 µm paraffin sections were baked in an incubator at 60°C for 1 hour. For deparaffinization, they were then placed in a glass coplin jar basket and were placed in a series of 11 jars for 10 minutes each containing different solutions in the order: Histochoice, Histochoice, 100% ethanol, 100% ethanol, 95% ethanol, 95% ethanol, 70% ethanol, 70% ethanol, 1 X phosphate buffered saline (PBS), 1 X 0.1% triton, and 1 X PBS. Antigen retrieval was completed using a previously described procedure (Nelson 2013). Slides were rinsed four times in 1 X PBS. Blocking was completed with 10% donkey serum in 3% bovine serum albumin (BSA) for approximately 1 hour. Primary antibody was applied and slides were incubated at 4°C overnight. Primary antibodies that were used in this study (table 1) include β-III tubulin, GFRα2, tyrosine hydroxylase, DAPI, cytokeratin 7 (K7), sodium/potassium ATPase (Na/K-ATPase), cytokeratin 5 (K5), aquaporin 5 (Aqp5), and smooth muscle α-actin (αSMA). After incubation in

primary antibody, slides were rinsed twice in 1 X PBS. Secondary antibody matching the primary antibody origin was applied at a dilution of 1:200 and was incubated at room temperature for one hour. Secondary antibodies used include antibodies for the Cy5 and Cy3 channels, included those that originated from either mouse, rat, goat, or rabbit and were selected according to their specificity for the various primary antibodies (Table 1). To prevent non-specific fluorescence when imaging past the four secondary antibody types, direct conjugate, or primary antibodies marked directly with a fluorescent tag, were used to prevent the use of further secondary antibodies. Slides were rinsed twice in 1 X PBS prior to staining with DAPI, followed by another two 1 X PBS rinses. Slides were then mounted with glycerol media and imaged on an Olympus IX81 microscope.

Target	Manufacturer	Catalog Number	Concentration (mg/mL)	Channel	Dilution
Tyrosine Hydroxylase	Millipore	AV152	0.08	Cy3	1:100
GFRa2	R&D Systems	AF429	0.20	Cy5	1:100
K5	Covance	LL039	0.49	DC-Cy3	1:100
B3 Tubulin	R&D Systems	LL015	0.33	DC-Cy5	1:100
K7	Abcam	LL019	0.32	DC-Cy 3	1:100
NaKATPase	Epitomics	LL014	0.20	DC-Cy5	1:100
SMA	Sigma	A2547	1-1.50	DC-Cy3	1:500
AQP5	Allimone	LL009	0.16	DC-Cy5	1:100

Donkey anti-goat F(ab)2 secondary antibody	Jackson IR	705-175-147	1.5	Cy5	1:200
Donkey anti-rabbit F(ab)2 secondary antibody	Jackson IR	711-165-152	1.5	Dy3	1:200

Table 1) Dilutions and channels used for primary and secondary antibody staining used in immunohistochemical staining. Antibodies used as direct conjugates (DC) created by GE denoted with in-house catalog numbers for Larsen Lab (LL). Secondary antibodies from Jackson IR used for GFRa2 and Tyrosine Hydroxylase.

Image Capturing

The images that were used for the quantification process were taken from a 104-spot tissue microarray (TMA). This microarray was arranged with the two types of mouse model, NOD and healthy, of various ages in a random arrangement with the intent that the blind counter (N.P.) would not have earlier knowledge of the origin of each spot with the addition of postnatal day one control mouse tissue as a staining control. This arrangement also helped to control for even staining of the tissue during processing of the stains during immunohistochemistry. In order to compare the differences between the SS-like NOD mouse model and the CD-1 control mouse model, we quantified immunohistochemical markers within the submandibular gland and lacrimal glands using antibody staining. As multiplexing was used for the imaging of this project, multiple markers could be imaged at the same time on the same section of tissue utilizing different channels that could be selected for with the microscope. For

each spot, up to three images were acquired, which included a DAPI image and could include up to two images for primary or secondary antibody staining. The antibody stains were assigned to either the Cy3 or Cy5 channels using the secondary antibodies for Cy3 and Cy5 that stained in those selected wavelengths.

Quantification Method for Autofluorescent Background Subtraction Using FIJI

For quantifying the immunohistochemical markers observed in various tissue sections, the computer software program FIJI, ImageJ, version 1.50i, was used to quantify the immunohistochemistry data for the markers examined in this study. All images, before being quantified, had to be processed to remove any autofluorescence naturally present in the tissue. This was done in Fiji using a process that first allowed for the removal of background autofluorescence based on subtraction of an image of the bleached tissue without antibody imaged at a matched exposure time. This bleached image was then subtracted from the fluorescent image. To begin autofluorescence image subtraction, I first opened the two images in FIJI, and then created a stack using the “images to stack” function. For image registration I used the function ¨Linear stack alignment with SIFT¨ to ensure the images were properly aligned. From here, I measured the average pixel intensity in the unstained image using the measure function and inserted the measurement that resulted into the calculator plus function under the K1 value, selecting the divide function to divide the stained image by the unstained. This effectively removed any background autofluorescence found in the stained image by spatially subtracting the pixels found in the unstained image from the stained image. I then

used the background subtraction function to process the image with a traditional 10 pixel rolling ball background subtraction in order to eliminate any residual background.

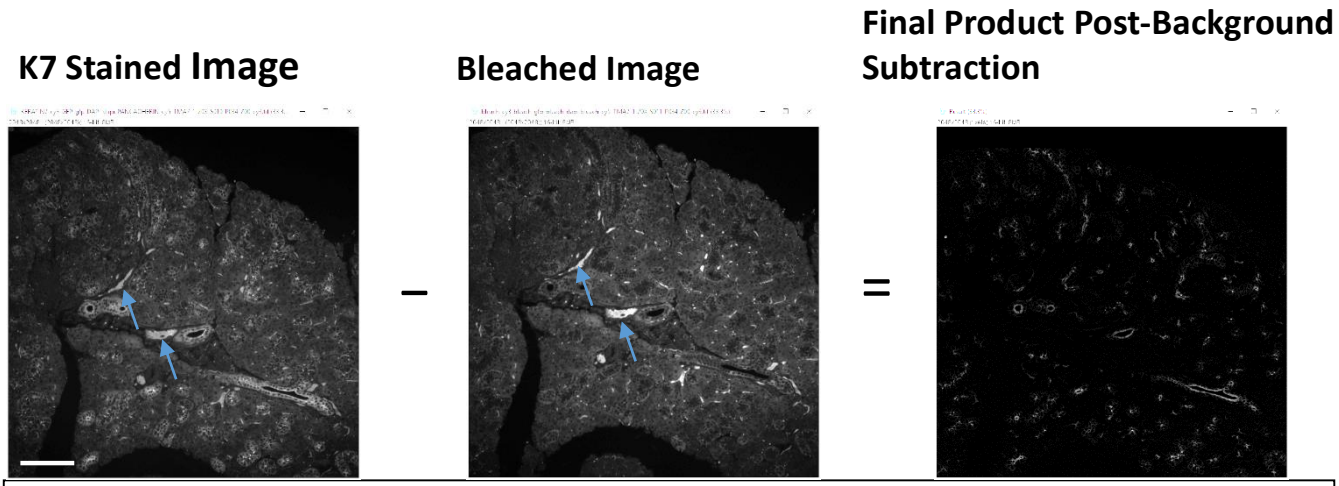

Fig 1. Subtraction of autofluorescence. Example of new method of autofluorescence image subtraction using FIJI (ImageJ 2). Note that while there is an inherent background (arrows) in each image, the K7 signal disappears after bleaching. Scale bar 100µm.

Rolling Ball Background Subtraction Method

All images, before being quantified had to be processed to remove any unnecessary background "noise". This was done through the program we used to quantify the images in the form of a background subtraction tool. I used the background subtraction function to process the image with a 50 pixel background subtraction. The type of background subtraction that ImageJ uses is described as a "rolling ball" background subtraction and removes the smooth continuous background, in this case to a radius of 50 pixels as the ball's dimension (Process May 2014).

ROI Immunohistochemistry Stain Quantification

I then chose five regions of interest (ROIs) within the epithelium as positively stained by epithelial cadherin (ECAD) on each spot quantified that I felt best represented the tissue as a whole. These regions of interest were uniform in the form of a square box with dimensions for the sides of 225 pixels. When converted to micrometers, this was the equivalent of 83.2 μm with an area of 6922.24 μm^2 per ROI. I then used the measure function to find the total pixels counted for ROIs. The next step was then averaging of ROI pixels per spot, followed by averaging the spots by mouse and then averaging these counts based on the conditions that the mice were subjected to. Results were then graphed with the standard error of the mean.

Overlay Quantification Method

To compare the co-localization of K5 and SMα-A in the epithelium using immunocytochemistry stained tissue microarray spots, the images of K5- and SMα-A-stained tissue spots were superimposed on each other so that areas stained by multiple markers could be quantified. Image overlays were created and processed using ImageJ 2 (FIJI v1.50i). Overlays were created using the "images to stacks" command, followed by registration using the plugin "Linear stack alignment with SIFT" using default parameters. Images were then separated from the stack using "stack to images" function. Background subtraction was performed at a value of 50 pixels followed by manual thresholding using the "threshold" function. Color overlays were created using red and green as original colors using the "color merge" function followed by the "invert" function in order to visualize the stains. For quantification, the blind counter first found the epithelial cadherin stain for the spot corresponding to the overlay and selected five ROIs of

225x225 pixels, taking care to avoid both edges of the tissue and areas that were not epithelium. These ROIs were then saved and an image of the overlay was opened. The regions were then selected individually, highlighting an area of the tissue and the plug-in “Color Inspector 3D” was opened for that region. From the drop down display option, “histogram” was selected, and the button labeled “LUT” was selected, measuring the overall pixels and percentage of the color by area of the region in a results window for black, red, green, and yellow. These colors correlated to unstained, SMα-A-positive, K5-positive, and SMα-A/K5-co-positive areas respectively. These measurements for each color were then copied and pasted into an excel sheet where the values for the five ROIs of each color per image were averaged with each other, yielding an average value per color per image. These values were then assigned to the mouse of origin (either NOD/ShiLtj or CD-1 control of either 18 or 22 weeks but labeled such that the blind counter would not have this knowledge) and values were averaged per mouse, then values were averaged per group of tissue origin. Graphs were produced in Microsoft Excel depicting group averages and standard error of the mean. This method provided average pixel counts of each color representing corresponding proteins separated by age and tissue type for comparison between groups.

RESULTS

Validation of Quantification Method Through Examination of Ductalization

To quantify the changes in epithelial marker expression between the NOD/ShiLtj SS disease model and healthy CD-1 control mice, we used comparative quantitative immunohistochemistry. We first examined the known ductal cell marker K7 (Nelson 2013), In the quantification of K7-stained images (Fig 2a), we observed a statistically significant increase in levels of K7 present. The level of K7 was significantly increased in the NOD/ShiLtj disease mouse model as compared to the CD-1 control mice in both the 18 and 22 week time points (Fig 2b). Statistical significance was determined using a student's two-tailed T-test with p-values values ≤ 0.05 and ≤ 0.001, respectively, as can be seen in figure 2b. The increase in K7 levels that I detected in the NOD/ShiLtj mouse is consistent with the ductalization that has been previously reported to occur in human SS (Konttinen 2006).

Aquaporin 5 Positive Epithelial Area is Decreased in the NOD/ShiLtJ Model

The correlation of levels of Aqp5 and expression patterns with salivary disease is controversial in the literature. We then quantified expression levels for images stained with AQP5 (Fig 2a), the marker for the acinar secretory cells, (Fig 2c) and observed decreasing levels of AQP5 in the disease models as compared to the CD-1 control models. The decrease in expression was not steep enough to be statistically significant, but persisted through both the 18 and 22 weeks age mice, suggesting a decreasing trend in reduction of acinar tissue in the SS disease model compared to the control tissue.

Given that ducts have been reported to increase and acinar cells have been reported to decrease with Sjogren's syndrome, we also quantified data comparing total epithelial area marked for by K7 and AQP5 in 22 week mice (Fig 2d). This provided data on the total epithelial area that was K7+ and AQP5+ in the NOD/ShiLtJ disease mice as compared to the CD-1 control mice, and we found them to significantly increase and decrease, respectively in the NOD/ShiLtJ model as compared to control.

Overall Epithelial Area is Unchanged in the NOD/ShiLtJ Model

To compare epithelial cell sub-populations against the whole epithelium, we wanted to find a protein that was not changed with disease. Na/K-ATPase is a membrane protein that we have used as a membrane marker in past studies (Nelson, 2013) that is expressed in many cells but is enriched in epithelial cells relative to mesenchyme cells in the salivary gland. When we stained for Na/K-ATPase and quantified images (Fig 2a), marking epithelial tissue as a whole, it was observed that there was no significant change in Na/K-ATPase in the NOD/ShiLtJ mouse model as compared to the CD-1 control model, as indicated by the p-values (Fig 2e). However, the graph demonstrates an increasing trend in expression of Na/K-ATPase in the 22 week NOD/ShiLtJ mice compared to the age-matched control mice (Fig 2e).

A

NaKATPase Aqp5 K7 DAPI

CD-1

NOD/ShiLtJ

18 Week

22 Week

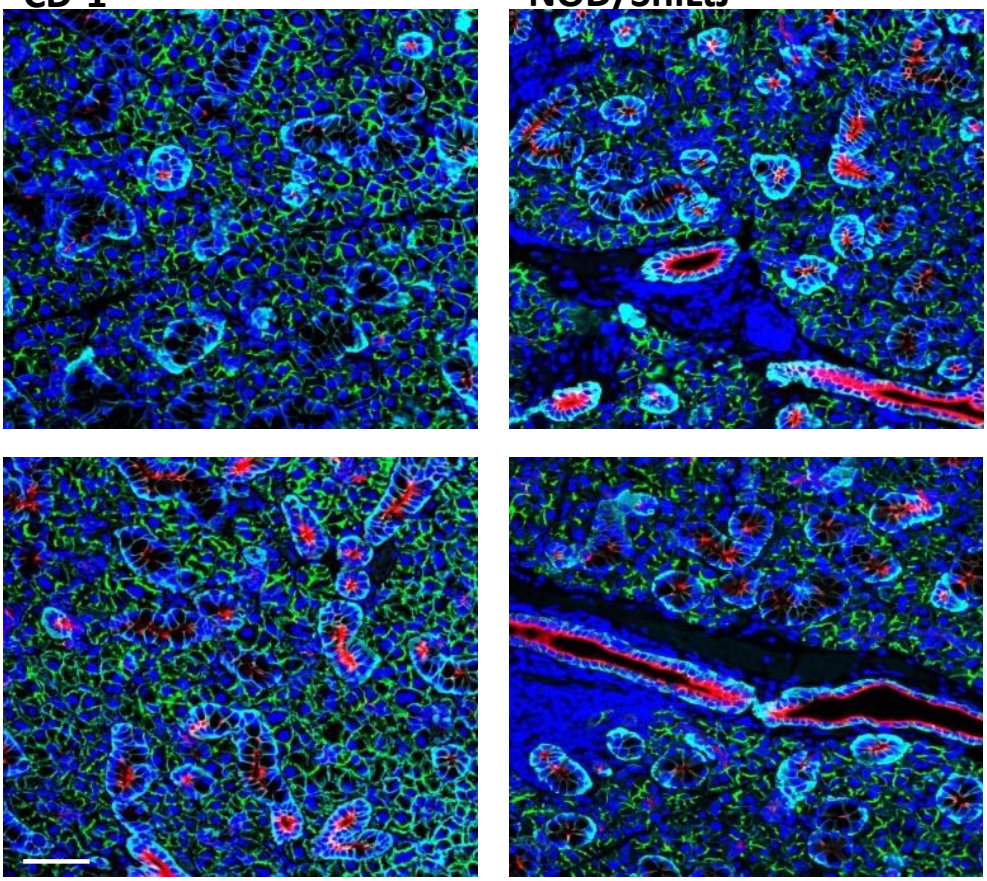

B

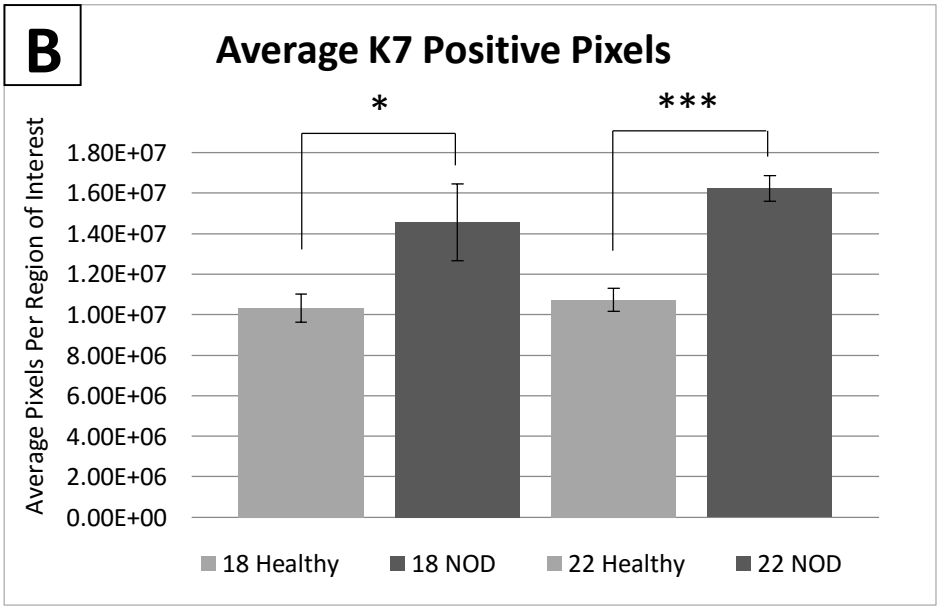

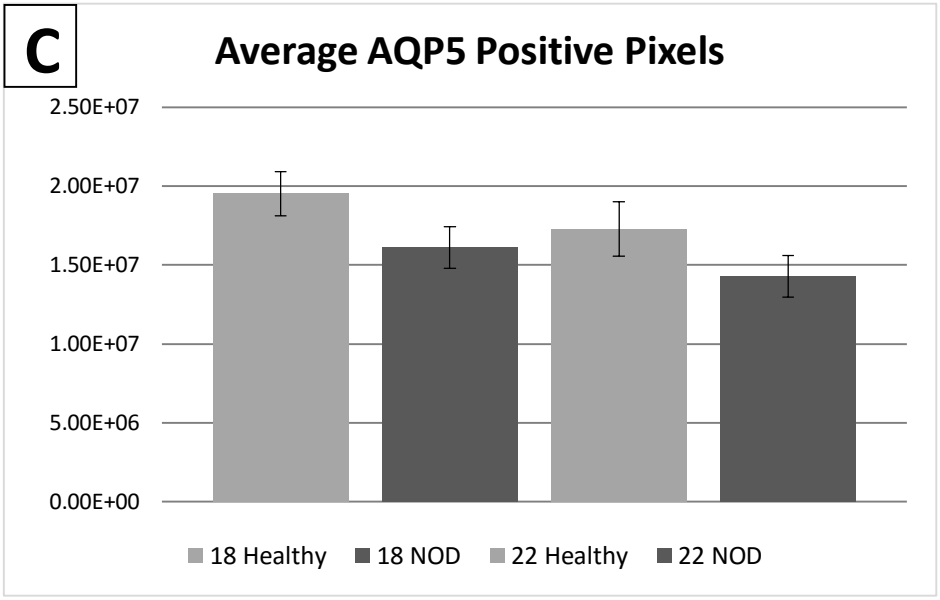
C
Average AQP5 Positive Pixels
2.50E+07
2.00E+07
1.50E+07
1.00E+07
5.00E+06
0.00E+00
18 Healthy
18 NOD
22 Healthy
22 NOD

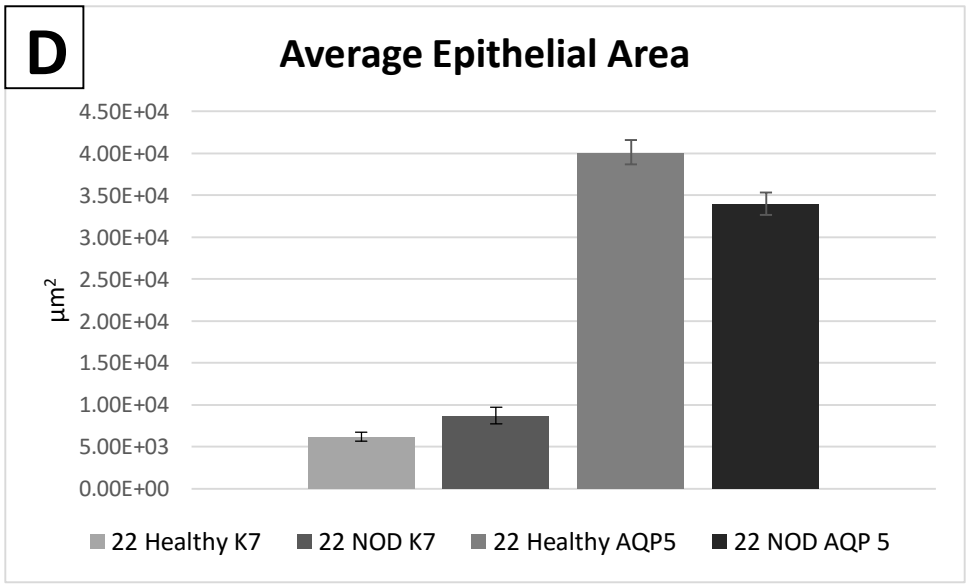
D
Average Epithelial Area
µm²
4.50E+04
4.00E+04
3.50E+04
3.00E+04
2.50E+04
2.00E+04
1.50E+04
1.00E+04
5.00E+03
0.00E+00
22 Healthy K7
22 NOD K7
22 Healthy AQP5
22 NOD AQP 5

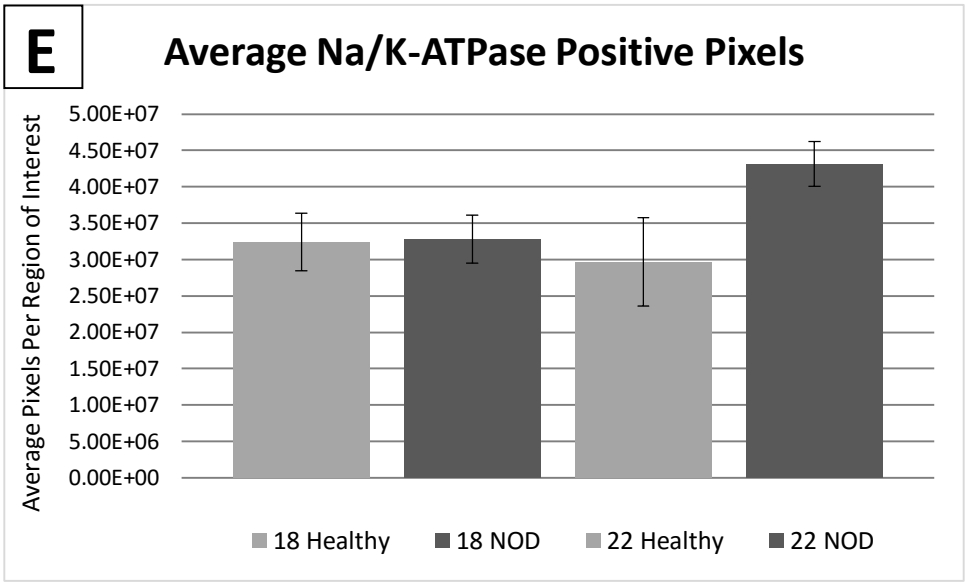

Fig 2. Ductalization and reduction of secretory epithelium occurs in the NOD/ShiLtJ mouse model. **a)** Increased K7 ductal cell marker expression was seen in NOD/ShiLtJ disease model tissue as compared to CD-1 control tissue in overlays of immunohistochemically stained images showing stains for DAPI, Na/K-ATPase, AQP5 and K7. Disease progression is shown using both 18 and 22 week old mice. **b)** Increased expression of K7 ductal marker in epithelial tissue of SMG in NOD/ShiLtJ as compared to control in both 18 and 22 week mice. **c)** There was a decreasing trend in expression of Aqp5 acinar cell marker in epithelial tissue of SMG in NOD/ShiLtJ as compared to control in both 18 and 22 week mice. **d)** Increased percentages of K7+ area and decreased percentages of AQP5+ area were found to be significant in 22 week mice NOD/ShiLtJ mice as compared to control mice. **e)** Constant levels of expression of Na/K-ATPase, an epithelial tissue marker, were seen in SMG tissue in NOD/ShiLtJ as compared to control in either 18 or 22 week mice. Student's two-tailed T-test *p≤0.05, **p≤0.01, ***p≤0.001, scale bar 100μm.

Smooth Muscle α-Actin is Increased in the NOD/ShiLtJ Model

As reduction in myoepithelial cells may contribute to glandular hypofunction in SS, we examined SMα-A-positive myoepithelial cells. On quantification of the stain for SMα-A (Fig 3a), a marker for myoepithelial cells, which surround the acinar cells and facilitate salivary secretion, interestingly, we noticed an increasing trend in SMa-A in 18 week NOD/ShiLtJ mice as compared to control that continued that reached significance at 22 weeks, correlating to a p-value ≤ 0.01 (Fig 3b).

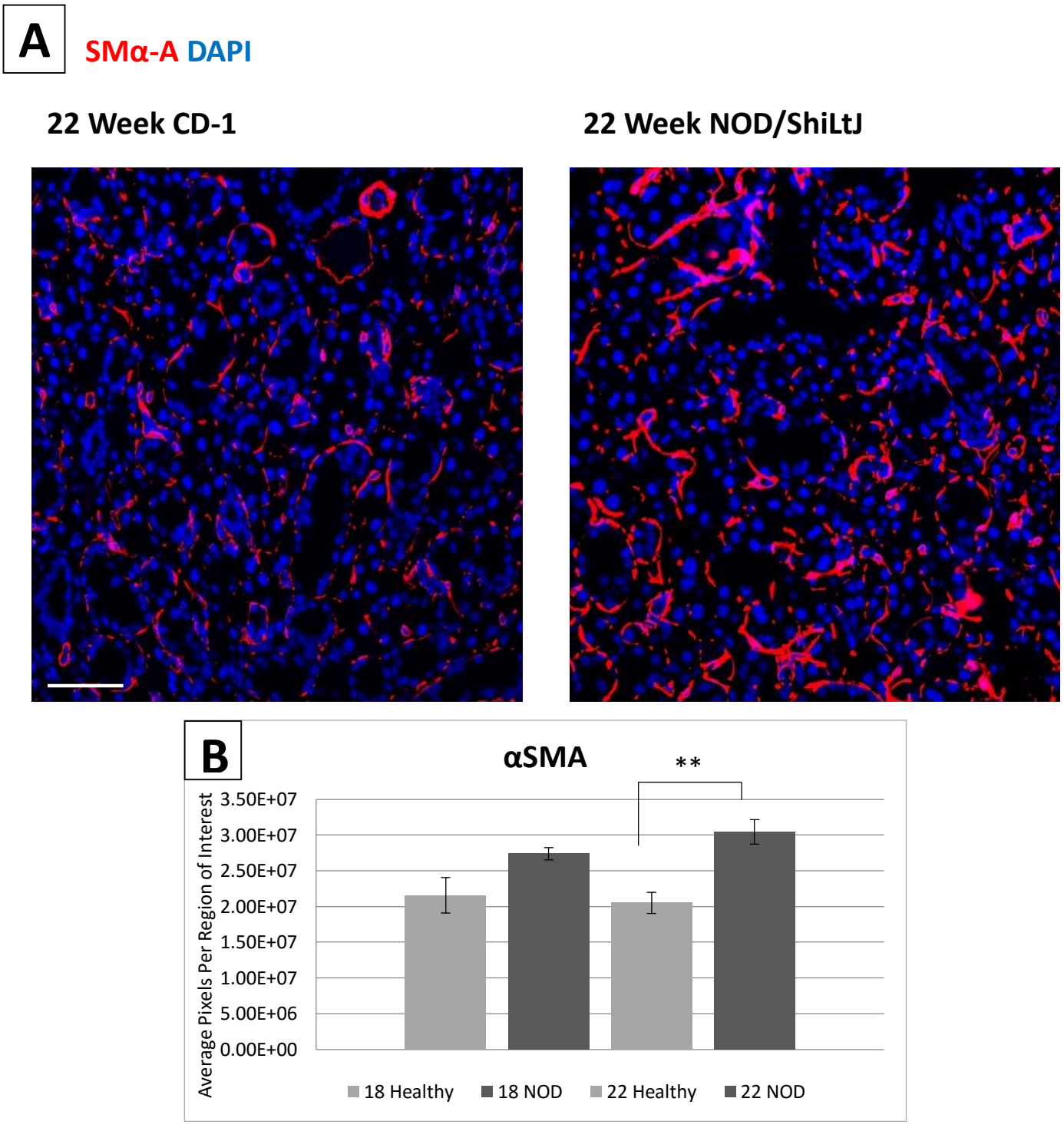

Fig 3. SMα-A-positive myoepithelial expression increases significantly in the 22 Week NOD/ShiLtJ model. a) Increased SMα-A expression in NOD/ShiLtJ as compared to control mice in overlays of immunohistochemically stained images marked for DAPI and SMα-A of tissue from 22 week mice. **b)** Levels of expression of SMα-A in epithelial tissue of SMG in NOD/ShiLtJ are significantly increased in the 22 week NOD/ShiLtJ mouse as compared to CD-1 control. Student's two-tailed T-test $p \leq 0.01$, scale bar 100µm.

Cytokeratin 5-Positive Progenitor Cells Are Increased in the NOD/ShiLtJ Model

Progenitor cells are required for development and regeneration; however, nothing is known regarding the progenitor cell populations in the NOD/ShiLtJ mouse. We therefore performed immunostaining to detect the progenitor marker K5 (Fig 4a), marking the epithelial progenitor cell population, and similarly to SMa-A, observed an increasing trend in the 18 week NOD/ShiLtJ mice, as compared to control that continued in the 22 week mice, reaching statistical significance with a p-value of ≤ 0.05 (Fig 4b).

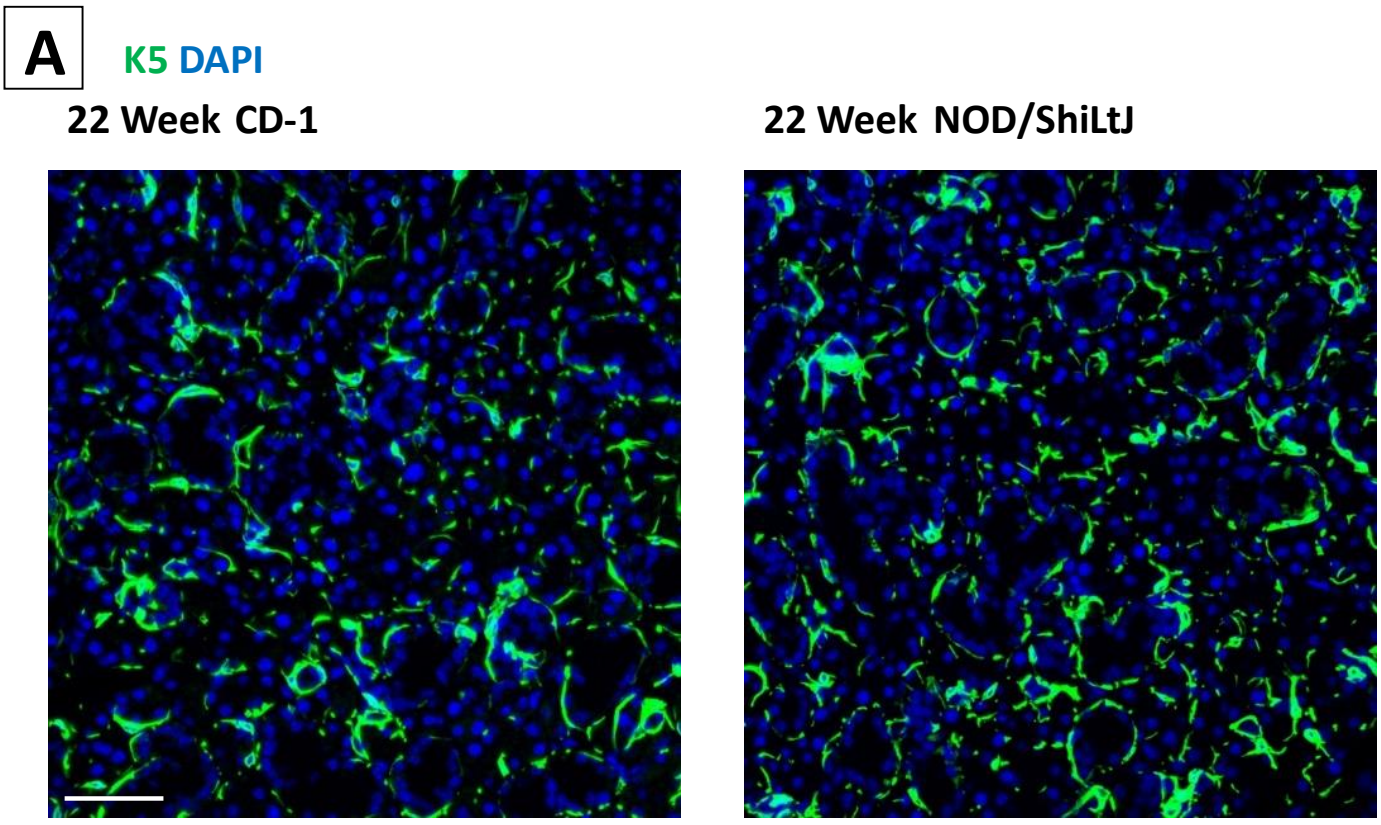

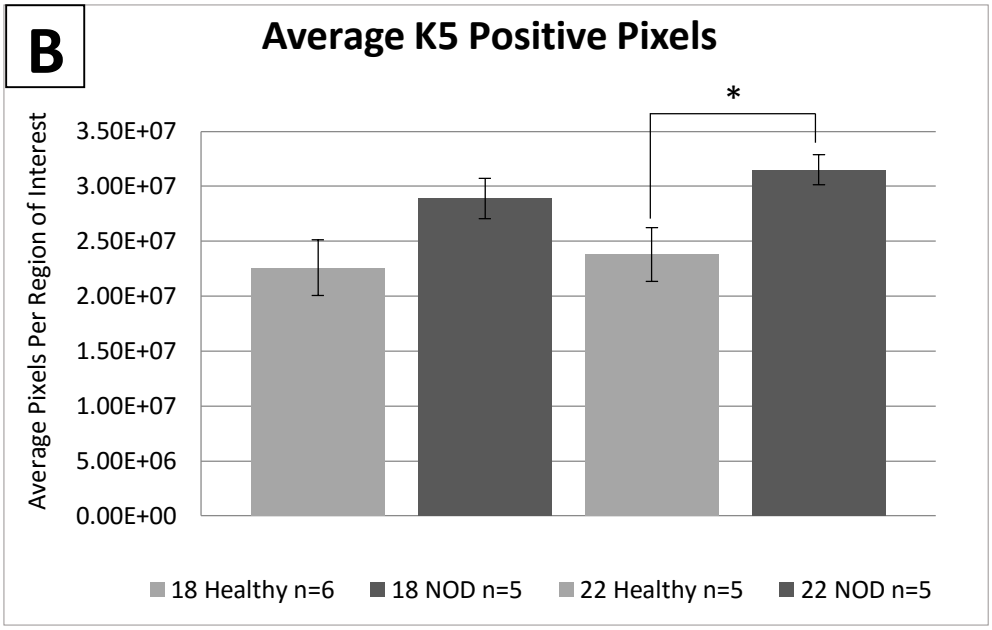

Fig 4. K5-positive progenitor levels increase similarly to SMα-A in the NOD/ShiLtJ model a) Increased K5-positive tissue expression in disease model as compared to control in overlays of immunohistochemically stained images showing stains for markers DAPI and K5 of tissue from 22 week mice. **b)** Levels of expression of K5 in epithelial tissue of SMG in NOD/ShiLtJ increase significantly at 22 weeks. Student's two-tailed T-test $p \leq 0.05$, scale bar 100µm.

Innervation is Increased in the NOD/ShiLtJ Model

In order to examine total innervation, we measured βIII-tubulin, and quantified the stained images (Fig 5a). We observed a significant increase in BIII-tubulin in the NOD/ShiLtJ model as compared to CD-1 control in both the 18 and 22 week mice, indicating an increase in total innervation within the SMG tissue. This increase correlated to p-values ≤0.05 for both the 18 and 22 week mice, as seen in figure 5b. Since βIII-tubulin is expressed by both sympathetic and parasympathetic innervation, this increase could represent an increase in either or both nerve cell populations.

To specifically examine sympathetic innervation, which negatively correlates with regeneration, we performed immunohistochemistry to detect tyrosine hydroxylase (TH) (Fig

5a). We observed a significant increase in TH levels in the NOD/ShiLtJ disease model as compared to CD-1 control in both the 18 and 22 week mice (Fig 5c). This increase was shown to be statistically significant with p-values ≤0.05 and ≤0.01 for 18 and 22 week mice, respectively.

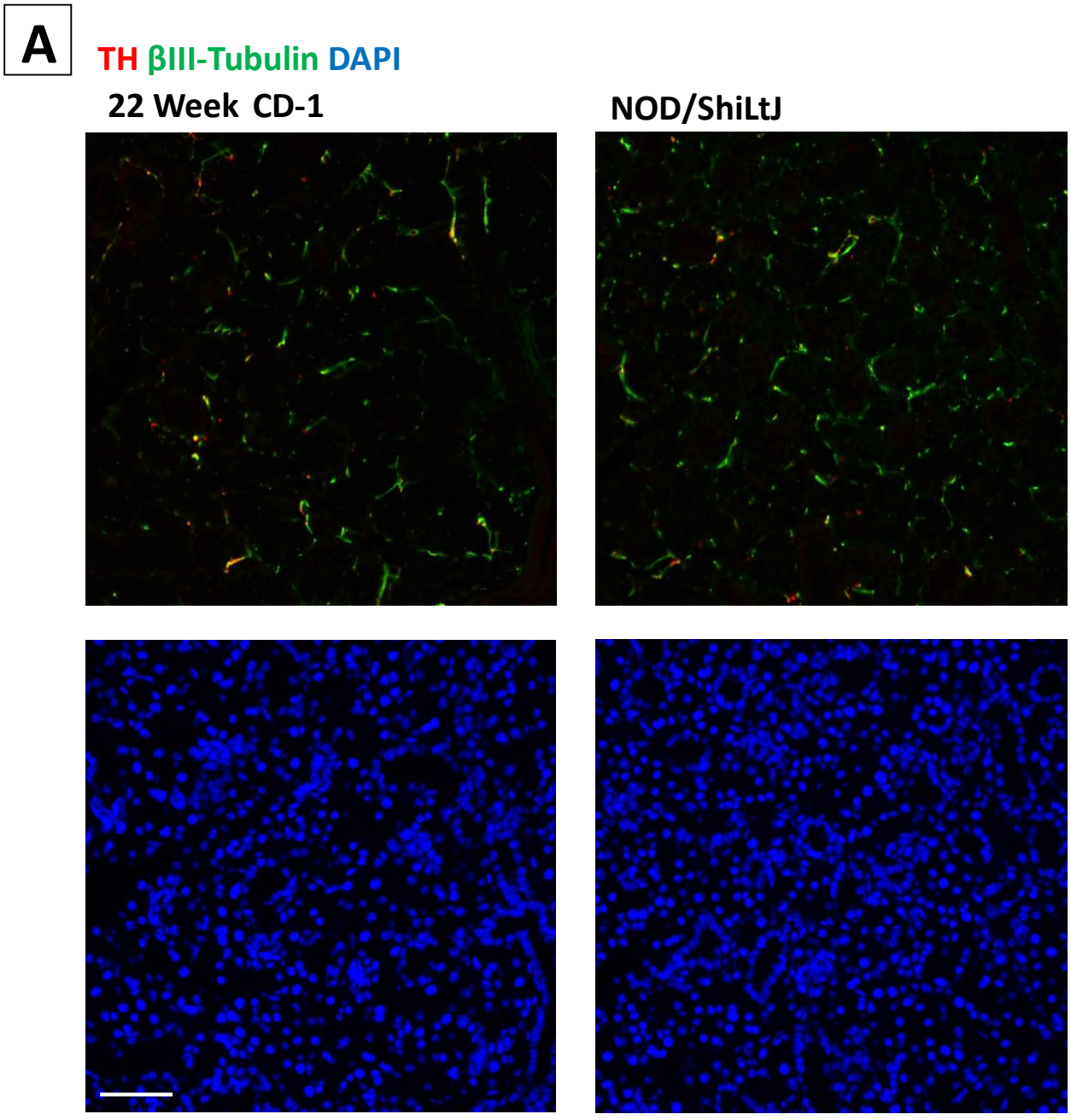

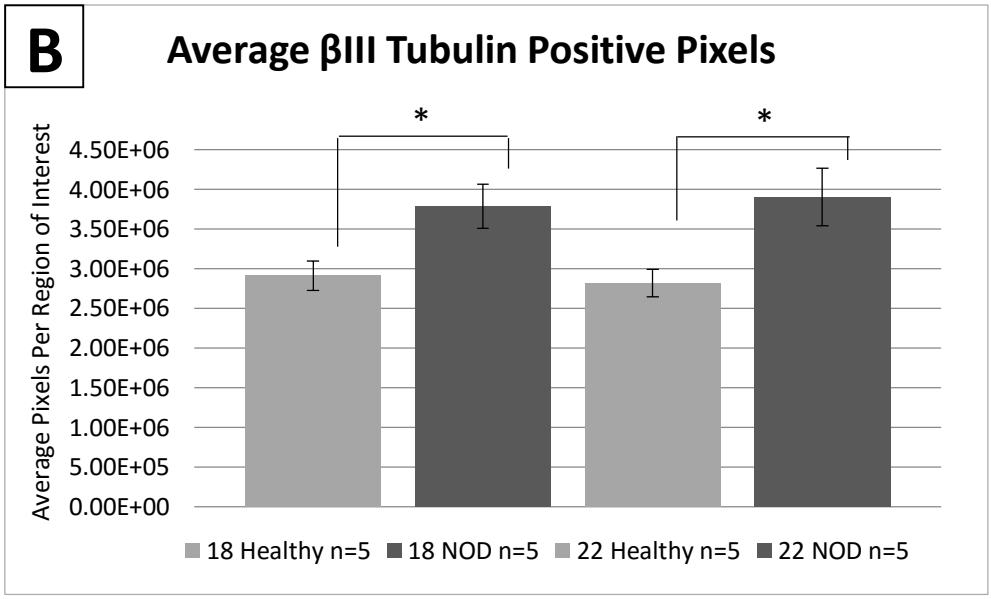

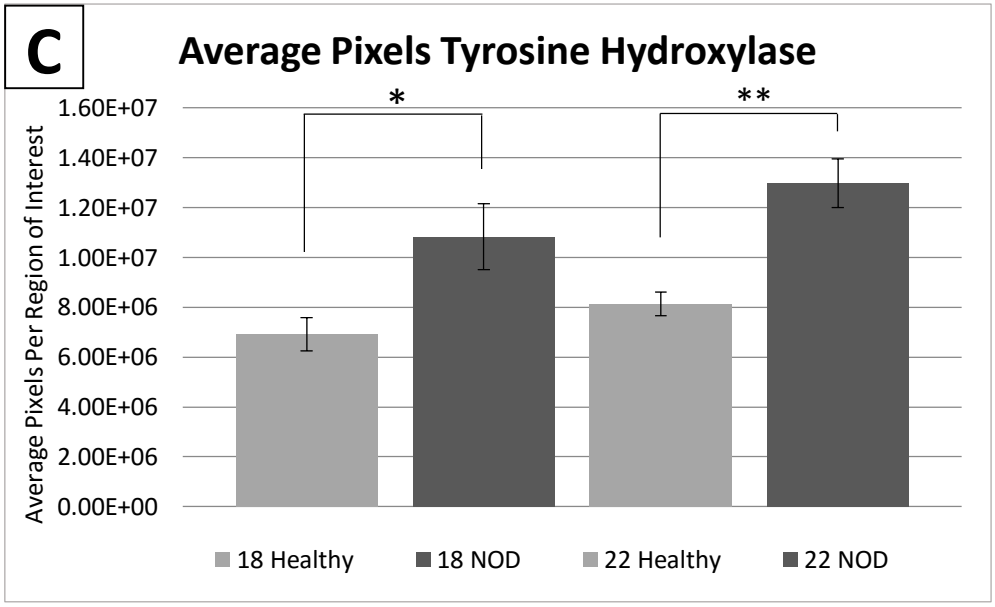

Fig 5. Increase in βIII tubulin-positive innervation coincides with an increase in tyrosine hydroxylase positive innervation in the NOD/ShiLtJ model. a) Increased expression of βIII tubulin and tyrosine hydroxylase in disease model mice as compared to control in overlay images immunohistochemically stained for markers DAPI, tyrosine hydroxylase, and βIII tubulin of tissue from 22 week mice. **b)** Statistically significant increase in levels of expression of βIII tubulin in epithelial tissue of SMG in NOD/ShiLtJ as compared to control in both 18 and 22 week mice, indicating an increase in overall innervation in glands. **c)** Tyrosine hydroxylase in epithelial tissue of SMG. Statistically significant increase in levels of expression of tyrosine hydroxylase in epithelial tissue of SMG in NOD/ShiLtJ as compared to control in both 18 and 22 week mice, indicating an increase in sympathetic innervation in glands. Student's two-tailed T-test *p≤0.05, **p≤0.01, scale bar 100μm.

To specifically examine parasympathetic innervation, we stained and imaged for Gfrα-2 (Fig 6a). We could qualitatively observe that there was an increase in the levels of Gfrα-2 in the NOD/ShiLtJ mice as compared to the CD-1 control at 22 weeks, but were unable to accurately quantify this stain due to the high background present in several of the images after numerous attempts at staining for this marker.

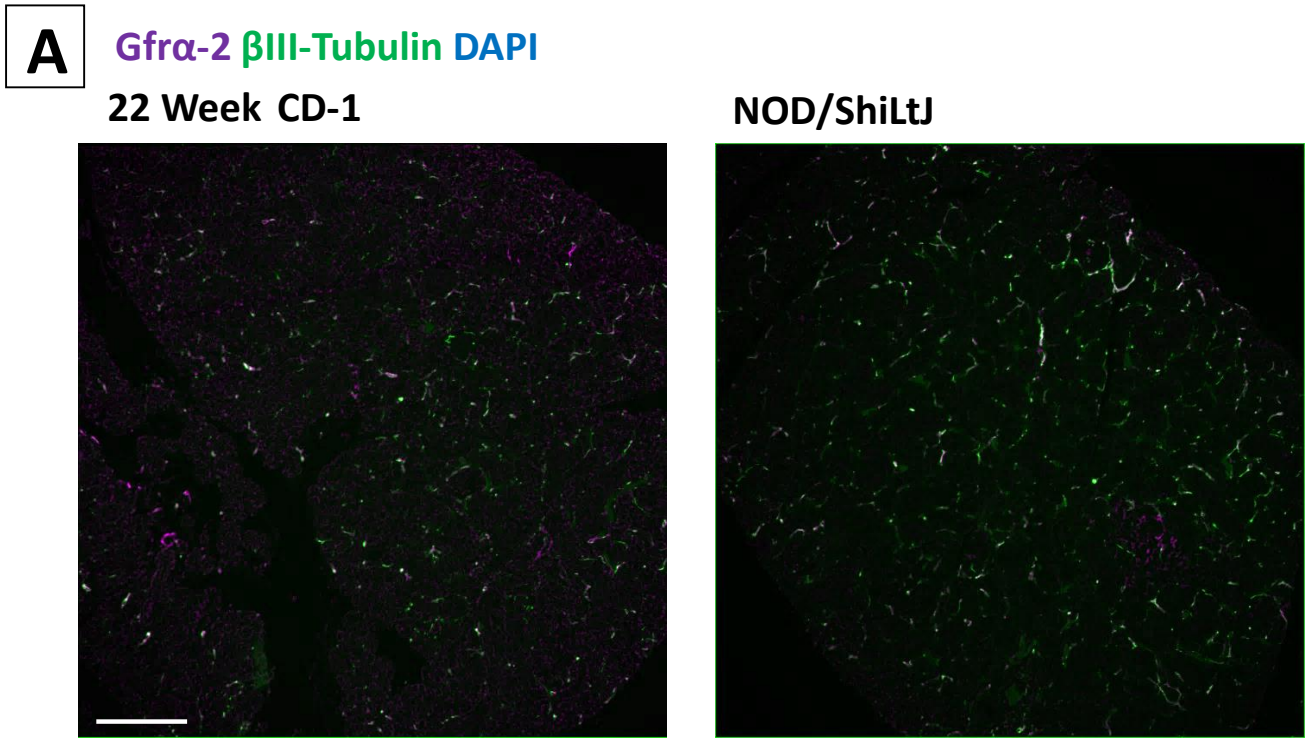

Fig 6. Gfrα-2-positive innervation also increases in the NOD/ShiLtJ model. a) Increased co-positive staining for Gfrα-2 and βIII tubulin in image overlays of tissue immunohistochemically stained for markers DAPI, Gfrα-2, and βIII tubulin from 22 week mice. Scale bar 100µm.

DISCUSSION

Increased Cytokeratin 7 Indicates Ductalization in the NOD/ShiLtJ Model

Since previous research shows that ducts increase within SS salivary tissue (Konttinen 2006), we used the quantification of ductal marker K7 as proof of concept for our method of quantification of epithelial markers. As expected, there was a statistically significant increase in K7 staining (Fig 2a) within the NOD/ShiLtJ mouse model SMG tissue as compared to CD-1 age-matched controls at both 18 and 22 weeks (Fig 2b), indicating that our method of quantification was indeed yielding accurate results. In order to examine tissue ductalization, we examined K7 positive epithelial area and found a significant increase in NOD/ShiLtJ mice as compared to control at 22 weeks. This increase in K7-positive epithelium indicates that the NOD/ShiLtJ tissue undergoes ductalization similarly to that reported in human SS previously (Konttinen 2006).

Aquaporin 5 Positive Epithelium Decreases as Ductalization Occurs

When we examined acinar cell marker AQP5 (Fig 2a) we observed that AQP5 levels decreased in the NOD/ShiLtJ mice as compared to the healthy controls. Although this trend was not statistically significant, it was present in both the 18 and 22 week time points. Since this finding could indicate a mild reduction in the acinar cell populations, we completed further analysis of AQP5-positive acinar epithelial area which indicated a significant decrease in AQP5 positive area in 22 week NOD/ShiLtJ mice as compared to controls. Although not specifically addressed in this study, decreased acinar cell populations as a function of disease presence may

indicate hyposalivation which may have contributed to the need for providing wet chow to the NOD/ShiLtJ mice.

Increased Smooth Muscle α-Actin Occurring in the NOD/ShiLtJ Model is Not Observed in Human Sjögren's Syndrome Tissues

Initially during our examination of myoepithelial marker SMα-A (Fig 3a), we hypothesized that we would see a decrease in expression due to the loss of regenerative ability and decreased glandular function as a factor of disease progression. If the gland could not repair or replace damaged myoepithelial cells, we expected the myoepithelial cell population to decrease. Instead, we observed increasing SMα-A expression in NOD/ShiLtJ mice as compared to control, becoming significant at 22 weeks (Fig 3b). Similar changes in SMα-A were not observed in human SS patients as compared to human controls (data not shown). It is possible that changes in myoepithelium occur earlier in the development of SS and due to the common late diagnosis of SS were not observed in human patients in this study.

Epithelial Progenitor Marker Cytokeratin 5 Increases With Disease Progression in the NOD/ShiLtJ Model

Since K5-positive progenitor cells have been reported to be able to contribute to all epithelial cell types n the embryonic gland (Knox 2010), we examined the levels of K5 present in the NOD/ShiLtJ model (Fig 4a). We expected the levels of K5 to decrease in the disease model as compared to control as a result of decreased function and decreased epithelial area coinciding with decreased regenerative capabilities of the tissue. Instead, however, we

observed an increase in K5 levels beginning at 18 weeks in the NOD/ShiLtJ model as compared to control that gained significance by 22 weeks (Fig 4b). Increased K5 levels were also present in human SS tissues as compared to control tissues (data not shown). It is possible that increased K5 levels in the NOD/ShiLtJ model reflect an increase in undifferentiated progenitor cells or a loss of cellular identity during disease progression.

In order to examine total epithelium, we quantified Na/K-ATPase and found no significant change in expression in the NOD/ShiLtJ disease model as compared to the CD-1 control model (Fig 2e). We did note a small, yet non-significant increase in Na/K-ATPase levels in the 22 week NOD/ShiLtJ model as compared to control, however, since Na/K-ATPase is expressed in ducts preferentially, we believe this to correlate with the increased expression of K7-positive ductal tissue seen in the NOD/ShiLtJ mice (Fig 2b).

Increased Innervation in the NOD/ShiLtJ Model

In order to examine total innervation within the salivary glands, we stained and quantified neuronal specific βIII tubulin (Fig 5a) and found an overall increase in innervation in NOD/ShiLtJ mice as compared to controls. βIII tubulin levels in the NOD/ShiLtJ model were significantly increased in both the 18 and 22 week mice (Fig 5b). In order to further characterize the increase in innervation, we stained and quantified sympathetic innervation marker tyrosine hydroxylase since sympathetic innervation has been shown to reduce regeneration in the salivary gland (Knox 2013). When comparing the results of quantification of βIII tubulin with those of tyrosine hydroxylase, we found there to be a correlation and that the expression of tyrosine hydroxylase also increased significantly in the NOD/ShiLtJ mice as compared to the CD-

1 controls in both the 18 and 22 week mice (Fig 5c). As increased sympathetic innervation is known to decrease regeneration within the adult SMG (Knox 2013), this may indicate a loss of regenerative ability in the NOD/ShiLtJ model. To further characterize changes in innervation, we also stained for parasympathetic innervation marker Gfrα-2 (Fig 6a), and we found a qualitative increase in expression of Gfrα-2 in the NOD/ShiLtJ mice as compared to the control mice at 22 weeks of age. As Gfrα-2 stains for parasympathetic innervation, we examined this marker in the hopes of being able to observe the ratio of parasympathetic to sympathetic innervation within both control and disease tissue. Due to stain quality, however, Gfrα-2 was not able to be examined quantitatively. This increase in Gfrα-2 expression, although we could not quantify to determine a ratio, may indicate increased parasympathetic innervation within the tissue which could lead to increased maintenance and expansion of the K5-positive progenitor cell population in accordance with the previously established relationship between K5-positive basal progenitors and parasympathetic innervation within the SMG (Knox 2010).

CONCLUSION AND SIGNIFICANCE

Overall, we observed that within the NOD/ShiLtJ SS disease model as compared to the CD-1 control mice, the expression of K7, SMα-A, and K5 increased, indicating an increase in ducts, myoepithelial cells, and basal progenitors, respectively. Increased K7 levels corresponded with increased K7-positive ductal areas of epithelium, while areas positive for the acinar marker AQP5 decreased. Basal progenitor marker K5 levels increased in the NOD/ShiLtJ model, a phenomena that was reflected in human SS tissue, which may reflect an expansion of progenitors or a dedifferentiation event due to disease state. Interestingly, increased SMα-A levels in the NOD/ShiLtJ model did not correspond with the decreased SMα-A levels in human SS tissues, likely due to the model reflecting an earlier state of disease progression than in commonly seen in human biopsy. In the NOD/ShiLtJ model, we also observed an increase in the overall innervation as marked with βIII tubulin, correlated with an increase in sympathetic innervation as marked by tyrosine hydroxylase within the SMG epithelium. We believe this increase in sympathetic innervation could contribute to a loss of function within the gland. The regenerative capabilities of the gland could be impeded through increased sympathetic innervation, which may provide a possible pathway to the treatment of the symptoms of SS, through examining further and finding methods to manipulate the innervation pathways within the salivary gland, influencing functional tissue development. Qualitative observations also suggested that there is an increase in parasympathetic innervation in the disease model as compared to the control model; however, further study would be necessary to elucidate the full extent of influence that both sympathetic and parasympathetic innervation have on the development of a functional salivary gland.

REFERENCES

1. Daniels, T.E. (1984) Labial salivary gland biopsy in Sjögren's Syndrome: assessment as a diagnostic criterion in 362 suspected cases. *Arthritis Rheumatology* (30):571–589.
2. Ferreira, João N., et al. (2013) Interactions between developing nerves and salivary glands. *Organogenesis* (9): 199-205
3. Fox, Philip C. (2007) Autoimmune diseases and Sjögren's Syndrome: an autoimmune excrinopathy. *Annals of the New York Academy of Sciences*: 15-21.
4. Gao, Juehua, et al. (2006) Sjögren's Syndrome in the NOD mouse model is an interleukin-4 time-dependent, antibody isotype-specific autoimmune disease. *Journal of Autoimmunity* (26): 90-103.
5. Holmberg, Kyle V., et al. (2014) Anatomy, biogenesis and regeneration of salivary glands. *Monographs in Oral Science: Saliva: Secretions and Functions* (24): 1–13.
6. Ihrler, Stephan, et al. (2000) Sjögren's Syndrome and MALT lymphomas of salivary glands: a DNA-cytometric and interphase-cytogenetic study. *Modern Pathology*: 4-12.
7. Jonsson, Malin V., et al. (2006) Impaired salivary gland function in NOD mice: association with changes in cytokine profile but not with histopathologic changes in the salivary gland. *Arthritis & Rheumatism* (54): 2300-2305.
8. Knox, Sarah M., et al. (2010) Parasympathetic innervation maintains epithelial progenitor cells during salivary organogenesis. *Science*: 1645-1647.
9. Knox, Sarah M., et al. (2013) Parasympathetic stimulation improves epithelial organ regeneration. *Nature Communications* (4): 1-7.

10. Konttinen, Yrjö T., et al. (2006) Immunohistopathology of Sjögren's Syndrome. *Autoimmunity Review* (6): 16-20.
11. Lavoie, Teagan N., et al. (2011) Current Concepts: Mouse models of Sjögren's Syndrome. *Journal of Biomedicine and Biotechnology*: 1-14.
12. Nelson, Deirdre A., et al. (2013) Quantitative single cell analysis of cell population dynamics during submandibular salivary gland development and differentiation. *Biology Open* (2): 439-447.
13. Proctor, Gordon B., et al. (2007) Regulation of salivary gland function by autonomic nerves. *Autonomic Neuroscience: Basic & Clinical* (133): 3-18.
14. "Process." *ImageJ User Guide*. National Institute of Health, n.d. Web. 1 May 2014. <http://rsbweb.nih.gov/ij/docs/guide/146-29.html#toc-Subsection-29.14>.
15. Shiboski, S.C., et al. (2012) American College of Rheumatology classification criteria for Sjögren's Syndrome: A Data-Driven, Expert Consensus Approach in the SICCA Cohort. *Arthritis Care Res (Hoboken)* (64): 475-487.
16. "Sjögren's Syndrome Foundation - Treatments." *Sjögren's Syndrome Foundation*. N.p., n.d. Web. 28 Apr. 2014. <https://www.sjogrens.org/home/about-sjogrens-syndrome/treatments>.
17. Tincani, Angela, et al. (2013) Novel aspects of Sjögren's Syndrome in 2012. *BMC Medicine* (11): 93
18. Tucker, A.S. (2007) Salivary gland development. *Seminars in Cell and Developmental Biology* (18):237–244.

19. Venables, Patrick J.W. (2004) Sjögren's Syndrome. *Best Practice Research Clinical Rheumatology* (18): 313-329.
20. Westhoff, G. (2010) Epidemiology of primary Sjögren's Syndrome. *Zeitschrift für Rheumatologie* (1): 41-49